Bedload transport measurements with impact plate geophones in two Austrian mountain streams (Fischbach and Ruetz): system calibration, grain size estimation, and environmental signal pick-up

Dieter Rickenmann[1], Bruno Fritschi[1]

[1]Swiss Federal Research Institute WSL, Birmensdorf, 8903, Switzerland

Correspondence to: Dieter Rickenmann (dieter.rickenmann@wsl.ch)

Abstract.

The Swiss plate geophone system is a bedload surrogate measuring technique that has been installed in more than 20 streams, primarily in the European Alps. Here we report about calibration measurements performed in two mountain streams in Austria. The Fischbach and Ruetz gravel–bed streams are characterized by important runoff and bedload transport during the snowmelt season. A total of 31 (Fischbach) and 21 (Ruetz) direct bedload samples were obtained during a six year period. Using the number of geophone impulses and total transported bedload mass for each measurement to derive a calibration function, results in a strong linear relation for the Fischbach, whereas there is only a poor linear calibration relation for the Ruetz measurements. Instead, using geophone impulse rates and bedload transport rates indicates that two power law relations best represent the Fischbach data, depending on transport intensity; for lower transport intensities, the same power law relation is also in reasonable agreement with the Ruetz data. These results are compared with data and findings from other field sites and flume studies. We further show that the observed coarsening of the grain size distribution with increasing bedload flux can be qualitatively reproduced from the geophone signal, when using the impulse counts along with amplitude information. Finally, we discuss implausible geophone impulse counts that were recorded during periods with smaller discharges without any bedload transport, and that are likely caused by vehicle movement very near to the measuring sites.

1 Introduction

In the past decade or so, an increasing number of studies were undertaken on bedload surrogate acoustic measuring techniques which were tested both in flume experiments and in field settings. A review of such indirect bedload transport measuring techniques was recently published by Rickenmann (2017a, 2017b). Examples of measuring systems include the Japanese pipe microphone (Mizuyama et al., 2010a, 2010b; Uchida et al. 2013; Goto et al. 2014), the Swiss plate geophone (Rickenmann and Fritschi, 2010, Rickenmann et al. 2012, 2014), other impact plate systems (Krein et al., 2008, 2016; Møen et al. 2010; Reid et al. 2007; Beylich and Laute 2014; Taskiris et al. 2014), and hydrophones, i.e. underwater microphones (Barton et al. 2010; Camenen et al. 2012; Rigby et al. 2015). It is well known that bedload transport rates often show very

large variability for given flow conditions (Gomez, 1991; Leopold and Emmett, 1997; Ryan and Dixon, 2008; Recking, 2010), and that prediction of (mean) bedload transport rates is still very challenging, particularly for steep and coarse–bedded streams (Bathurst et al., 1987; Nitsche et al., 2011; Schneider et al. 2015, 2016). For such conditions, direct bedload transport measurements are typically difficult to obtain, or may be impossible to make during high flow conditions (Gray et al., 2010). In contrast, indirect bedload transport measuring methods have the advantage of providing continuous monitoring data both in time and over a cross–sections, even during difficult flow conditions, and are therefore expected to increase our understanding of bedload transport.

A fair number of these measuring techniques have been successfully calibrated for total bedload flux, which generally requires contemporaneous direct bedload transport measurements in the field (Thorne, 1985, 1986; Voulgaris et al., 1995; Rickenmann and McArdell, 2007, 2008; Mizuyama et al. 2010b; Rickenmann et al. 2014; Mao et al., 2016; Habersack et al., 2017; Kreisler et al., 2017). Essentially, linear or power law relations were established between a simple metric characterizing the acoustic signal and bedload mass. In some studies further calibration relations were established to identify particle size, either based on signal amplitude (Mao et al., 2016; Wyss et al., 2016a) and/or on characteristic frequency of that part of the signal which is associated with a single impact of a particle (e.g. for impact plate systems; Wyss et al., 2016b) or by determining a characteristic frequency for an entire grain size mixture (for the hydrophone system; Barrière et al., 2015a). A few of the acoustic measuring techniques were used to determine bedload transport by grain size classes (Mao et al., 2016; Wyss et al., 2016a). Finally, some studies examined to what extent findings from flume experiments can be quantitatively transferred and applied to field sites for which independent, direct calibration measurements exist (Mao et al., 2016; Wyss et al., 2016b, 2016c).

In this study we report on calibration measurements of the Swiss plate geophone (SPG) system in two mountain streams in Austria. The Fischbach and Ruetz gravel–bed streams are characterized by important runoff and bedload transport during the snowmelt season. During a six year period, 31 (Fischbach) and 21 (Ruetz) direct bedload samples were obtained in the two streams, respectively. The objectives of this paper are: (i) to present and discuss different ways of analysing the geophone calibration measurements, also in comparison with data and findings from other field sites and flume studies; (ii) to show that the observed coarsening of the grain size distribution with increasing bedload flux can be qualitatively reproduced from the geophone signal; and (iii) to discuss implausible geophone impulse counts that were recorded during periods with small discharge and without any bedload transport, and that are probably associated with close–by vehicle movement.

2 Field sites and calibration measurements

2.1 Overview of field sites and geophone measurements

The first indirect bedload transport measurements using impact plates were made in the Erlenbach from 1986 to 1999 using a piezoelectric crystal as sensor, with the aim of continuously monitoring the intensity of bedload transport and its relation to

stream discharge (Bänziger and Burch, 1990; Rickenmann, 1994, 1997; Hegg et al., 2006; Rickenmann and McArdell, 2007). A geophone sensor was used at the Erlenbach and at all other field sites that were set up in the year 2000 and later (Rickenmann and Fritschi, 2010). In the meantime, the SPG system has been installed in more than 20 streams primarily in Central Europe (Rickenmann, 2017b). An array of steel plates is typically installed flush with the surface of a sill or check dam, a location where there is only a small chance for (substantial) deposition of bedload grains during transport conditions.

The Fischbach and Ruetz field sites were installed by the Tyrolean Hydropower Company (TIWAG). They are located in partly glaciated catchments in the Tyrolean Alps (Fig. 1), at elevations of 1544 m a.s.l. (Fischbach) and 1688 m a.s.l. (Ruetz). Thus, the streams have a nival and glacial runoff regime, with typical daily discharge variations and regular bedload transport during snow and glacier melt in spring and summer. At both field sites, water discharge and bedload transport have been monitored since 2008. The stream cross–section is essentially trapezoidal at both measuring sites, with the banks protected by riprap and inclined at 45° (Fig. 2, 3). The geophone sensors are fixed in a cylindrical aluminium case and are mounted on the underside and in the middle of stainless steel plates, which are screwed into supporting steel constructions (UPN profiles) and are acoustically isolated by elastomer elements. The steel plates are 0.360 m long, 0.496 m wide, and 0.015 m thick. The entire steel construction is 8.2 m long (transvers to the flow direction) and embedded into a concrete sill, founded two meters into the river bed. The entire concrete structure is 8.7 m wide, and it is laterally inclined at 5% to the river left side (Fig. 3), which improves the discharge measurements at low flows. The steel plates are horizontal in flow direction (no longitudinal slope). The sill is protected with riprap on the up- and downstream side. Starting with the first steel plate located 0.35 m from the right bank, every second steel plate is equipped with a geophone sensor, so that there are a total of eight sensors at each site. The riprap on the downstream side of the sill is inclined at about 15% over a length of about 2 m.

At both sites, the concrete sill is located 4 m downstream of the cross–section where flow stage is measured on the left side of the stream, and where flow velocity measurements are made by TIWAG to establish a flow rating curve. At the Fischbach, a bridge crosses the stream some 13 m upstream of the concrete sill, and provides vehicle access to the measuring hut on the left side on a small forest road with very infrequent traffic. Along the right side of the stream a local paved road passes nearby, situated only in 5 m horizontal and about 4.5 m vertical distance above the concrete sill with the geophone plates (Fig. 3). Uphill the road leads to the village of Gries with about 200 inhabitants. This is the only village to be accessed upstream of the measuring site. In winter it serves as a relatively small ski resort. At the Ruetz, a bridge crosses the stream some 15 m upstream of the concrete sill, and provides vehicle access to a large parking lot, paved with gravel, on both sides of the stream. The measuring site is located at Mutterbergalm in the Stubai valley. From there a cable car provides access to a large skiing area (winter) and to a hiking area (summer) in the mountains. The public road ends at Mutterbergalm. The parking lot is situated in a similar minimal distance to the measuring cross section as at the Fischbach, i.e. with about 5 m horizontal and 4.5 m to 5 m vertical distance above the concrete sill. This information is important for the analysis and interpretation of the pick-up of geophone signal by environmental sources other than bedload transport.

2.2 Direct bedload measurements for system calibration

At each of the two sites, a streamlined metal pillar was installed 0.5 m downstream of the plate with the geophone sensor no. 5 to facilitate the calibration measurements. The metal pillar has a height of 2.5 m and a maximum width of 0.25 m and ensures that a pressure–difference type metal basket sampler fits snugly onto the bed and can be held in place during the bedload sampling operation (Fig. 2b). The aperture of the basket is 50 cm by 50 cm, the same width as the sensor plate. The basket has a notch (cut–out) at a downstream distance of 0.45 m from the aperture (Fig. S1, Supporting information). The notch is somewhat larger than the cross–section of the metal pillar, and the inside of the notch is equipped with rollers. This system allows an exact positioning of the basket during geophone calibration measurements. The maximum width of the basket is 0.90 m and the total length is 2.10 m. During operation the upper surface of the sampler is horizontal while the lower surface is declined at 15% in the downstream direction, in line with the artificial bed in the vicinity of the metal pillar. Over the 0.80 m tail–end of the sampler, the top and sidewall surfaces of the basket are made of 10 mm metal wire mesh. The total volume of the basket is about 0.91 m^3.

The calibration measurements used here were obtained by TIWAG in both streams during the summer months of 2008 – 2013 using the basket bedload sampler. A total of 31 measurements from the Fischbach and 21 measurements from the Ruetz were used in this analysis (Table 1). The maximum sample mass caught in the sampler was 518 kg (including particles finer than 10 mm) in the Fischbach; assuming a bulk density of 1600 kg m^{-3}, the bedload volume of this sample was about 0.32 m^3 or about a third of the total sampler volume. Four calibration measurements from the Fischbach could not be used due to overfilling of the sampler. The grain size distribution of the samples was determined by sieve analysis by a TIWAG– owned engineering consultant. A line–by–number analysis was performed in both streams in October 2012 to estimate the grain size distribution of the bed surface upstream of the geophone sites (Fig. 4).

The sampling duration of the calibration measurements was essentially selected according to bedload transport intensity. For very high bedload transport rates, the sampler may be quickly filled; ideally, sampling should be stopped before the basket is full (to avoid scouring of previously caught particles and to reduce uncertainty about the exact filling time). For very small bedload transport rates, the total sampled mass may be relatively small for a fixed sampling duration; if only few particles travel over the steel plate, the variability of the signal response is larger, due to random factors influencing the signal response (e.g. different transport modes and impact locations) that only tend to average out for larger numbers of particles that moved over the plate (see also beginning of Discussion section below). Therefore we used generally longer sampling durations for lower transport rates.

2.3 Signal pre–processing, recorded geophone values, and amplitude histogram analysis

The bedload impact shocks on the steel plate are transmitted to the geophone sensor and, thereby, an electrical potential is produced. The standard geophone sensor uses a magnet in a coil as an inductive element. The magnet picks up the vibrations of the steel plate and induces a current in the coil which is proportional to the velocity of the magnet. Whenever the voltage

127 exceeds a preselected threshold amplitude value, $A_{\min}$, the shock is recorded as an impulse, *IMP*. Contrary to all the other

128 sites equipped with an SPG system, the threshold amplitude value $A_{\min}$ used to determine *IMP* values was set at 0.07 V at the

129 Fischbach and Ruetz (Tables 2, 3). The reason is that the first regular geophone recordings in the Fischbach had shown

130 maximum amplitudes in excess of 10 V, the upper limit of the recording system. To increase the resolution of large

131 amplitudes, the raw signal was dampened by about 30%. To compensate for lower signal strength in relation to the impulse

132 counts, the threshold amplitude value $A_{\min}$ was also reduced by 30% when compared with a typical value of 0.1 V used at

133 other sites.

134   At most of the field sites with SPG measurements, several signal summary values were routinely stored in the past. The

135 most often used summary value for calibration purposes are the summed impulse counts *IMP*. These values were found to

136 correlate reasonably well with bedload mass or volume transported (Rickenmann and McArdell, 2007, 2008; Rickenmann et

137 al., 2012, 2014). Another useful summary value is maximum amplitude *MaxA* that may be determined for different recording

138 intervals. During calibration measurements, all summary values were typically stored in 1 second intervals. During normal

139 flow monitoring, the recording interval for the summary values at the Fischbach and Ruetz was 15 minutes. (At other SPG

140 measurement sites operated by WSL this recording interval is typically 1 minute).

141   Using the so–called amplitude histograms (AH), Wyss et al. (2016, 2014) demonstrated for the SPG measurements at the

142 Erlenbach (Swiss Prealps) that absolute bedload masses for each grain size class could be successfully calculated for both the

143 calibration and validation data obtained with the moving basket samplers. The continuous recording of AH data was also

144 implemented at the Fischbach and Ruetz measuring sites, with a recording interval of 1 minute. At these sites, impulses were

145 determined separately for 17 amplitude classes as listed in Table 2. For the analysis in this study, for each amplitude

146 threshold value A_{th} (upper class boundary value) a corresponding particle size *D* was estimated according to an empirical

147 relation given in Wyss et al. (2016c, Eq. 11) and reported in Appendix A as Eq. (A1).

148 **3. Results**

149 **3.1 Calibration relations for bedload mass and bedload flux using impulse counts**

150 The following calibration relations and calibration coefficients were determined using the transported bedload mass *M*, for

151 particles with *D* larger than 10 mm, the impulses *IMP* summed over the sampling period of duration T_s:

152    $M = k_{\text{lin}}\ IMP$ (1)

153    $M = k_{\text{pow}}\ IMP^e$ (2)

154    $k_{\text{tot}} = \Sigma M / \Sigma IMP$ (3)

155 where the units are in [kg] for *M* and for the coefficients (k_{lin}, k_{pow}, k_{tot}), and the Σ sign implies a summation over all the

156 calibration measurements per site. Equations (1) and (2) were obtained from a linear regression (using log values in case of

Eq. 2), while Eq. (3) represents a mean, linear calibration coefficient based on the total mass and the total number of impulses for all calibration measurements taken together. The resulting coefficients (k_{lin}, k_{pow}, k_{tot}), exponents (e) and statistical properties of the calibration relations are reported in Table 3. The squared correlation coefficient r^2 was determined between the measured masses M and the estimated masses M_{reg} (using eq. 1, 2, or k_{tot} in eq. 2). The relative standard deviation $s_{e,r}$ is determined for the ratios (M_{reg}/M), using the regression relation to determine M_{reg} from the recorded impulses IMP.

For the Fischbach, the calibration relations in the form of Eqs. (1) and (2) show a rather high correlation coefficient (Fig. 5, Table 3), which is also characteristic for similar calibration relations determined for the Erlenbach (Rickenmann et al., 2012, 2014). For the Ruetz, the calibration relations in the form of Eqs. (1) and (2) are less well defined (Fig. 6, Table 3). Due to the inclusion of four additional calibration measurements obtained in 2012 and 2013, the correlation coefficient for the Ruetz is lower than in an earlier analysis that used only 17 measurements from the period 2008 to 2011 (Rickenmann et al., 2014). This level of correlation is similar to calibration measurements obtained for the Navisence stream in Switzerland (Wyss et al., 2016c) for which most measured bedload masses were smaller than 20 kg; for the Ruetz, 15 out of 21 calibration measurements also have bedload masses smaller than 20 kg. Using the k_{tot} coefficient from Eq. (3) in Eq. (1) results in very similar statistical properties as compared to using k_{lin} in Eq. (1); while the relative standard deviation $s_{e,r}$ is very similar for the Fischbach in both cases, it is about 25% larger for the Ruetz when using the k_{tot} coefficient as compared to using the k_{lin} coefficient (Table 3).

Systematic flume experiments were performed for different grain size classes to investigate the dependence of a linear calibration coefficient, defined as $k_{bj} = IMP/M$, on grain size D (Wyss et al., 2016b). This study used bedload particles from four streams including the Ruetz and Fischbach, and it was found that k_{bj} values showed a local maximum at a grain size D of around 40 mm, in agreement with earlier flume experiments using quartz spheres of different diameters (Rickenmann et al., 2014). Therefore, we analysed the field calibration measurements from the Ruetz and Fischbach in a similar way (Fig. 7), and these data essentially confirmed the findings from the flume experiments. The bedload samples from the Ruetz and Fischbach show a general tendency for D_{84} to increase with increasing unit bedload transport rate q_b (Fig. 8), where D_{84} is the grain size for which 84 % of material by weight are finer (determined for particles with $D > 10$ mm). It is therefore not surprising that k_{bj} values also exhibit a local maximum when plotted against the impulse rate, $IMPT$ (Fig. 9), which is a proxy for transport rate, and where $IMPT = IMP/(T_s\, w_p)$, with the plate width $w_p = 0.5$ m. Finally this lead us to determine alternative calibrations in terms of unit bedload transport rate per plate width $q_{b,p}$ as a function of impulse rate, $IMPT$ (Fig. 10), with a limiting value of around 0.5 to 1 (0.5^{-1} m^{-1} s^{-1}) to separate the two ranges with a different power law function:

$$q_{b,p} = a_1\, IMPT^{b1} \qquad \text{for } IMPT < 0.48\ (0.5^{-1}\ \text{m}^{-1}\ \text{s}^{-1}) \tag{4}$$

$$q_{b,p} = a_2\, IMPT^{b2} \qquad \text{for } IMPT > 0.48\ (0.5^{-1}\ \text{m}^{-1}\ \text{s}^{-1}) \tag{5}$$

where the units for $q_{b,p}$ are in (kg 0.5^{-1} m^{-1} s^{-1}) and for $IMPT$ in (0.5^{-1} m^{-1} s^{-1}), and the coefficients and exponents are given in Table 3. Here, we determined $q_{b,p}$ and $IMPT$ deliberately per unit width of one plate since using the traditional 1 m unit

190 width would result in different coefficients a_1 and a_2 (and a different threshold value *IMPT* separating the application range

191 of Eq. 4 and Eq. 5), which would entail the risk of erroneous transformations of measured *IMPT* values into $q_{b,p}$ values for

192 each plate. In Table 3 we used the same coefficients and exponents (a_1, b_1, and a_2, b_2, respectively) for both stream sites. The

193 reason for this is evident from Figure 9. For the lower bedload transport or impulse rates (range of validity of Eq. 4), the

194 calibration measurements from the two streams show a very similar trend. For the higher bedload transport or impulse rates

195 (range of validity of Eq. 5), there are only calibration measurements from the Fischbach. The basic assumption hereby is that

196 Equations (4) and (5) are valid for both streams.

197   In Fig. 10, the regression relation for higher impulse rates was derived based on 14 calibration measurements from the

198 Fischbach with *IMPT* > 1 [(1/0.5) m^{-1} s^{-1}]. Similarly, the regression relation for lower impulse rates was derived based on 17

199 measurements from the Fischbach and 19 measurements from the Ruetz, all with *IMPT* < 1 [(1/0.5) m^{-1} s^{-1}]. The two power

200 law relations intersect at *IMPT* = 0.48 [(1/0.5) m^{-1} s^{-1}]. Using this limiting value, they were applied to the Fischbach and

201 Ruetz data, resulting in the statistical properties of the calibration relations (4) and (5) as reported in Table 3. It appears that

202 the data from both channel sites can be described reasonably well with these calibrations relations, the relative standard

203 deviation $s_{e,r}$ being about 98% for the higher impulse rates and about 110% for the higher impulse rates (Table 3). If Eqs.

204 (4) and (5) are applied to all calibration measurements of each stream separately, the clearly better statistical properties result

205 for the Fischbach (r^2 = 0.97, $s_{e,r}$ = 61 %) than for the Ruetz (r^2 = 0.50, $s_{e,r}$ = 145 %). In comparison to the calibration relation

206 determined with Eq. (2) for the Fischbach, Eqs. (4) and (5) will predict larger bedload transport rates for very small or very

207 large *IMPT* values (Fig. 10).

3.2 Coarsening of grain sizes with increasing bedload flux reflected in geophone signal

209 The amplitude histograms (AH data) for each calibration measurement were used to estimate grain size distributions (GSD)

210 for the basket sampler measurements, which were then compared with the sieve analyses of the bedload samples. For the

211 analysis of the AH data, the lowest class with impulses for A_{max} < 0.056 V was excluded, as this class represents

212 predominantly signal noise. For the remaining 16 classes the sum of the impulses per amplitude class was determined for all

213 1 min time steps for the duration T_s. This resulted in the proportion of impulses per amplitude class per calibration

214 measurement, not yet weighted for grain size. The impulses per class were weighted by the geometric mean diameter of each

215 class (Table 2) to the 2nd power, D_m^2, to estimate the cumulative distribution of AH-values; this weighting procedure

216 corresponds essentially to the method of Wyss et al. (2016), which is summarized in Appendix A. It is also noted that the

217 start (and end) time of the bedload sampling does not exactly correspond to the start (and end) time of the recorded AH data,

218 which introduced a further (generally minor) uncertainty when interpolating AH data for the first and last recording time step

219 of each bedload sampling period. For the results shown in Figures 10 and 11, the GSD was averaged for given classes of unit

220 bedload transport rates q_b, assigning the same weight to each measurement in a given q_b class. Bedload transport classes and

221 corresponding abbreviation names are defined in Fig. 11 and 12.

For the bedload samples from both Fischbach and Ruetz a general coarsening trend of the grain size distribution (GSD) with increasing unit bedload transport rate q_b can be observed, in agreement with general bedload transport theory (Parker, 2008). However, GSDs from individual calibration measurements are quite variable within given classes of q_b, both for the bedload samples and for the estimated GSD from the AH values, and do not necessarily follow the general trend. The GSDs estimated from the AH values generally show a qualitatively similar trend as the GSDs from the direct bedload samples, but with a limited quantitative agreement between the two methods.

For the Fischbach (Fig. 11) it is noted that only 2 calibration samples were available for the class Fi1, and these had the 2 smallest bedload masses (with 19 and 8 kg, respectively); this may be a reason for the poor agreement between estimated and measured GSDs. Similarly, the largest q_b class Fi4 for the Fischbach includes only 1 bedload sample. For the Ruetz (Fig. 12) we note that for the classes Ru1 and Ru3 the bedload masses were relatively small, including only 5 to 6 kg. Together with a small number of bedload samples (3 and 2, respectively), this may again be one reason for the relatively poor agreement between estimated and measured GSDs. In contrast, the bedload masses for the Ruetz for the class Ru2 (11 to 23 kg) and Ru4 (15 to 129 kg) were clearly larger.

3.3 Environmental noise pick-up of the geophone signal

Both measuring stations are situated at a relatively high elevation, and the stream catchments include mountain peaks with elevations above 3000 m a.s.l. Therefore the runoff during the winter period is very low, with a base flow below 0.6 m^3 s^{-1} at the Fischbach and below 0.3 m^3 s^{-1} at the Ruetz. During such flow conditions, only about half or two thirds of the sill with the steel plates is submerged under water (Fig. 2, Fig. S2). However, during winter geophone impulses are regularly recorded at all the geophone sensors in both streams (Fig. 13, Fig. 14). According to hydraulic calculations and observations the sill becomes fully submerged for flows of about 2.5 m^3 s^{-1} at the Fischbach and about 2.0 m^3 s^{-1} at the Ruetz. Therefore it is unlikely that these geophone impulses are the result of bedload transport.

For the Fischbach and the discharge classes smaller than 3 m^3 s^{-1} the mean IMP values per 15 minutes (IMP_{15}) vary between about 0.3 and 2.0. A similar analysis as in Fig. 13 but with a finer discharge resolution (classes of 0.25 m^3 s^{-1}) is presented in Fig. S3. It is also obvious that plates (sensors) no. 1 to 3 generally recorded more impulses than the other plates no. 4 to 8 (Fig. 13, Fig. S3), which is unlikely a result of bedload transport. For discharges up to about 3 m^3 s^{-1} traffic noise appears to be a likely source of the geophone impulses, since the local road passes on the river right side very close to the plates no. 1 to 3 (Fig. 2). For discharge classes larger than 4 m^3 s^{-1} the plates no. 4 to 8 (which have a larger water depth than plates no. 1 to 3) start to record more impulses on average (IMP_{15}) than plates no. 1 to 3; in addition the IMP_{15} values start to increase with increasing discharge (Fig. 13, Fig. S3). This behaviour is more in line with expectations from bedload–transport induced signals.

For the Ruetz and the discharge classes smaller than 1.0 m^3 s^{-1} the mean IMP_{15} values vary between about 0.2 and 2.0. Plates no. 5 to 8 generally recorded more impulses than the other plates no. 1 to 4 (Fig. 14, Fig. S4). The plates no. 1 to 3 are typically not submerged during these flow conditions, and no signal is to be expected from bedload transport. Again, traffic

noise appears to be a likely source of the measured geophone impulses. The plates on the river left side (5 to 8) tend to register more impulses on average because the access road to the parking lot passes on this side, hence more parking traffic is to be expected. A clearer dominance of the plates no. 5 to 8 (which have a larger water depth than plates no. 1 to 4) becomes apparent for discharge classes larger than about 1.5 m^3 s^{-1} at the Ruetz (Fig. 14, Fig. S4), which is in line with expectations from bedload–transport induced signals. The mean value of IMP_{15} averaged over all eight plates becomes larger than about 2 for discharges larger than roughly 2.0 m^3 s^{-1}, and above this discharge level the IMP_{15} values start to increase in general with increasing discharge.

To further investigate the potential source of the implausible geophone recordings, we classified the measured IMP_{15} values into 15 minute intervals during each day–time (Figs. S5, S6). For both streams and low flows, there is a clear daily cycle of geophone impulse activity although discharge remains rather constant during the entire day. This pattern clearly is present for the Fischbach for discharges Q smaller than about 3 m^3 s^{-1} and for the Ruetz for Q smaller than about 1.5 m^3 s^{-1}. Geophone activity is higher during the afternoon and the first half of the night at the Fischbach, and primarily during day time at the Ruetz. A clear absence of this or a similar daily pattern is evident for the Fischbach for Q larger than about 6 m^3 s^{-1} and for the Ruetz for Q larger than about 3.5 m^3 s^{-1} (Fig. S5, S6). This is a further indication that the geophone impulses at smaller discharges are mainly traffic induced. Taken together, the above analysis and interpretation suggests that bedload transport may be the dominant source of producing geophone impulses above a critical discharge Q_c of about 3.5 m^3 s^{-1} at the Fischbach, and above a Q_c of about 1.5 m^3 s^{-1} at the Ruetz.

Turowski et al. (2011) analysed the start and end of bedload transport in gravel-bed streams, including geophone measurements from the Fischbach and Ruetz for the years 2008 and 2009. They determined discharge values at the start (Q_s) and at the end (Q_e) of a transport period for the Fischbach and the Ruetz streams. The Q_s and the Q_e values that are smaller than the Q_c values identified in this study for the two streams, respectively, may contain implausible impulse counts. It is estimated that Turowski et al. (2011) used about 62 % (out of 95 measurements) potentially implausible values for the Fischbach and about 41 % (out of 492 measurements) potentially implausible values for the Ruetz. If these values were discarded from their analysis, this would change the histograms of the discharge at the start and end of transport for the two streams but it would not affect the general conclusions of the study of Turowski et al. (2011).

4. Discussion

4.1 Calibration relations for the Swiss plate geophone system and grain size determination

For a system such as the Swiss plate geophone it is known that the signal response depends on factors such as grain size, fluid or particle velocity, particle shape and mode of transport (i.e. sliding, rolling, saltating), and impact angle and impact location on the steel plate (e.g. Wyss et al., 2016b; Rickenmann, 2017b). For a given stream we may assume that the most of these factors vary within a given range, and the linear calibration coefficients primarily vary with flow conditions. Therefore, we expect that the mean signal response from a given particle size traveling over the plate becomes more stable the larger is

287 the total number of particles that have been transported over the plate. This is the main reason why we have primarily
288 considered the summed geophone summary values in the past (e.g. Rickenmann et al., 2012, 2014). Calibration
289 measurements from various sites confirmed the expectation that random factors influencing the signal response tend to be
290 more averaged out for longer integration periods (Rickenmann and McArdell, 2007, 2008; Rickenmann et al., 2012, 2014;
291 Wyss et al., 2016a, 2016c).

292   However, it may also be interesting to consider calibration relations for example between bedload rates and impulse
293 rates. If a linear calibration relation in the form of Eq. (1) is generally valid, a division of M and IMP by the sampling
294 duration T_s to determine rates will typically result in similar values for the linear calibration coefficient. Having performed
295 this alternative analysis in terms of bedload rates and impulse rates for the data of this study, two distinctly different ranges
296 of geophone signal response were found based on the data from the Fischbach (Fig. 10). These calibration measurements
297 suggest that two power law calibration relations in terms of rates provide a better fit than a single linear calibration relation
298 for the entire domain. The existence of two different ranges is likely a result of a changing GSD with increasing bedload
299 transport rates. We therefore also plotted data from calibration measurements at many other sites (Fig. 15), but no clear trend
300 for a similar pattern can be observed for most of these sites. The only exception is the Urslau stream in Austria; the
301 individual calibration measurements for this stream indicate a trend for a power law relation between q_b and $IMPT$ with an
302 exponent b < 1 for smaller q_b values and with an exponent b > 1 for lager q_b values (Kreisler et al., 2017). These calibration
303 measurements cover a range of about three orders of magnitude of q_b values; however different methods were used to obtain
304 the bedload samples for smaller and larger bedload transport intensities, and for the smaller range of q_b values the number of
305 measurements is limited.

306   For extreme flow conditions and very high bedload transport rates, there may be some limitations to extrapolating
307 calibration relations for the SPG system from the typical range of conditions investigated so far. Using the same steel impact
308 plates, we had installed piezoelectric bedload impact sensors (PBIS) in an earlier study to make bedload measurements at a
309 water intake of the Pitzbach mountain stream in Austria during two summer periods (Rickenmann and McArdell, 2008).
310 Impulses were counted in a similar way as for the Swiss plate geophone system. At the Tyrolean weir a total of 12 steel
311 plates with sensors were installed, with a natural gravel-bed surface upstream of the sill of 6 m width. Pressure sensors in the
312 settling basin downstream of the Tyrolean weir provided direct measurements of bedload volumes for calibration.
313 Downstream of the settling basin there is a flushing canal, where 3 steel plates with sensors were installed at the end of a 1.5
314 m wide and relatively smooth concrete channel. Flushing of sediment from the settling basin occurred over relatively short
315 time periods and thus produced high velocity flows and much higher bedload concentrations in the flow than at the (natural)
316 approach flow to the Tyrolean weir. While a reasonably well defined calibration relation could be obtained for the
317 measurements at the Tyrolean weir (Rickenmann and McArdell, 2008), a very large scatter was observed for the calibration
318 data of the flushing canal, for bedload volumes smaller than 100 m^3 (Fig. S9). This observation indicates that there are
319 limitations for the SPG system for extreme flow conditions. There is also evidence from debris-flow observations at the
320 Illgraben torrent in Switzerland with a geophone sensor mounted underneath a large steel plate (McArdell et al., 2007) that

the calibration relations for the SPG system obtained for bedload transport cannot be directly applied to estimate the mass of debris flows. A somewhat similar limitation was observed for the Japanese pipe microphone system, for which signal "saturation" may occur for high bedload transport rates, probably because this system is more sensitive to particle sizes smaller than 10 mm as compared to the SPG system (Wyss et al, 2016a; Rickenmann, 2017a, 2017b).

We used the AH data recorded during the calibration measurements at the Fischbach and Ruetz to estimate the transported bedload mass for each calibration measurement, M_{est}, by applying the procedure presented by Wyss et al. (2016a). This method is summarized in Appendix A, and it was specifically developed for the measuring conditions at the Erlenbach stream in Switzerland. Here, we used Eq. (A3) with the coefficient and exponent determined from the Erlenbach measurements; the relation of Eq. (A3) is expected to vary somewhat from site to site, and its application here is therefore associated with uncertainty. To assess the performance of this procedure when applied to the Fischbach and Ruetz, we plotted the ratio of estimated to observed bedload mass, M_{est}/M, as a function of bedload transport rate per plate $q_{b,p}$ and of observed mass M (Fig. 16). There is generally an over–estimation of bedload mass, up to a factor of about 10. Interestingly, the over–estimation decreases with increasing bedload transport rate (Fig. 16a). This result is in agreement with Fig. 15, which suggests that site–specific differences for calibration relations in terms of bedload transport rates and impulse rates tend to be relatively smaller for higher values of q_b. The degree of over–estimation of bedload mass as well as the scatter around a mean trend line for both streams appears to decrease also with increasing bedload mass for the data of the Fischbach and Ruetz (Fig. 16b), but this trend is somewhat less pronounced. Concerning grain size estimation from bedload surrogate measuring techniques, it may be noted that only a few other acoustic measuring techniques were (partly) successful in determining bedload transport by grain size classes from field measurements (Barrière et al., 2015b, using an impact plate hydrophone system; Mao et al., 2016, using a Japanese impact pipe microphone system).

To illustrate the uncertainty associated with using different calibration relations, we determined the yearly bedload (*YBL*) for 2010, which represents the year with the largest peak discharges and the largest *YBL* values (Table 4) for the period 2008–2013. For both streams, the *YBL* values are larger when using Eqs. (4) and (5) as compared to using Eq. (1); this is not surprising when comparing the linear with the power law calibration relations in Fig. 10. The power law calibration relations result in a 66 % higher *YBL* for the Fischbach and in a 85 % higher *YBL* for the Ruetz, if only plausible *IMP* values for discharges larger than Q_c are considered; the differences are larger if the entire *IMP* data set for 2010 is considered, including many implausible values recorded during low flow periods (Table 4). The between–stream comparison shows a much larger *YBL* for the Fischbach than for the Ruetz, which is due to more frequent peak discharges in the Fischbach exceeding about 10 m^3 s^{-1} during the year 2010 (Fig. S7, S8).

Based on the analysis of the GSD of all bedload samples we found on average a coarsening of the GSD with increasing bedload transport intensity (Figures 8, 11). However, GSDs from individual bedload samples are quite variable within given classes of bedload transport rates. The same is true if GSDs of the bedload samples are analysed in terms of changing discharge. The bedload samples were taken too randomly in time and too infrequently over the six years study period as to allow to examine whether there is any hysteresis trend for daily discharge cycles or over the entire summer season. In a

355 follow-up study, possible hysteresis trends were investigated based on the continuous geophone data which were converted
356 into bedload fluxes using equations (4) and (5), and the related findings are discussed in a forthcoming paper.

4.2 Environmental noise pick-up of the geophone signal

358 Hydrophones (underwater microphones) have been used to monitor bedload transport both in riverine and in coastal
359 environments (e.g. Thorne, 1990; Camenen et al. 2012; Basset et al., 2013). The objective of using such a system is to record
360 self–generated noise produced by collisions of moving bedload particles against each other or against the bed. The
361 application of this bedload surrogate measuring system can be impaired by other sources of noise, which may be caused by
362 vessel traffic, marine seismic exploration, or underwater military operations. If the main interest is in the acoustic signal due
363 to bedload transport, discounting for other sources of noise may be challenging and will also depend for example on the
364 spatial distance and the dominant frequencies of the different acoustic sources (Hildebrand, 2009; Etter, 2012; Basset et al.,
365 2013).

366 For the application of impact plates with acoustic sensors installed in a streambed there is very few experience with non-
367 bedload transport related sources of noise that may compromise their usefulness. We have shown in section 3.3 that road
368 traffic is a likely source of environmental noise producing a similarly strong signal at the SPG system as low–intensity
369 bedload transport during periods with moderate discharges. This observation was made for our two study streams Fischbach
370 and Ruetz, where in both cases the stream bed runs very close–by to roads, which are located only about half the stream–
371 width away from the edge of the bed. We have checked the impulse counts recorded for SPG systems installed at mountain
372 streams in Switzerland, particularly for low flow periods during winter time. There were generally very few impulses
373 recorded at these sites, indicating that road traffic is not an important source of noise. At these sites roads with regular traffic
374 are situated clearly farther away from the channel profile than at the two Austrian sites of this study: at the Navisence stream
375 in Zinal (Ancey et al., 2015) about 45 m (or 3 times the stream width), at the Albula River in Tiefencastel (Rickenmann et
376 al., accepted) about 30 m (or twice the stream width) to a road or about 15 m to a parking lot of a single building, and at the
377 Avançon de Nant stream near Pont de Nant about 20 m (or 4 times the stream width). The SPG system at the Erlenbach
378 stream in Switzerland (Rickenmann et al., 2012) is situated about 45 m away from a road; at this site we observed
379 implausible impulse counts limited to very short time periods that were likely due to hikers or possibly game passing at the
380 site.

381 At the Riedbach stream in Switzerland the geophone measuring site is situated at a water intake at an elevation of 1800 m
382 a.s.l, with few direct sunshine and often freezing temperatures during winter time. The access road ends at the water intake
383 and is not open to the public. For a seven year period from 2009 to 2015 geophone measurements showed no systematic
384 relationship between IMP and Q for discharges Q smaller than about 0.4 m^3 s^{-1}, but a considerable number of IMP were
385 recorded for Q values as small as 0.05 m^3 s^{-1} (Schneider et al., 2016). These discharge conditions are typical for the winter
386 period, and it was hypothesized that ice transport or break-up may be mainly responsible for the impulse counts. Impulses
387 may be typically as high as between 1 and 100 impulses for all seven plates and for 10 minute recording intervals.

388   Calculating a mean impulse value per plate for $Q < 0.3$ m^3 s^{-1} and including also zero values, this results in an average

389   duration of about 5 hours for one impulse to be registered at the Riedbach by one of the seven steel plates. This relatively

390   low occurrence frequency does not contradict the ice transport or break-up hypothesis.

391   **5. Conclusions**

392   The Fischbach and Ruetz gravel–bed streams are characterized by important runoff and bedload transport during the

393   snowmelt season. As a bedload surrogate measuring technique, the Swiss plate geophone (SPG) system has been installed in

394   2007 in both streams. During the six year period 2008 – 2013, 31(Fischbach) and 21 (Ruetz) direct bedload samples were

395   obtained in the two streams, and these measurements were analysed to obtain calibration relations for the SPG system at the

396   two sites.

397   As applied at many other SPG sites in the past, we first established calibration relations using total transported bedload

398   mass and the number of geophone impulses. A second way of analysing the geophone calibration measurements consisted in

399   using bedload transport rates and geophone impulse rates. For the Fischbach the second approach resulted in two power law

400   calibration relations, with different coefficients and exponents for small and large transport rates. The exponent was smaller

401   than one for small transport rates, and larger than one for larger transport rates. For the Ruetz data with essentially only

402   lower transport intensities, the power law relation derived from the Fischbach is also in reasonable agreement with the Ruetz

403   calibration measurements. The non-linear power law calibration relations are in qualitative agreement with the observed

404   coarsening of the bedload with increasing transport rates. According to findings from flume studies the signal response per

405   unit bedload mass increases for small grains up to grain size of approximately 40 mm, and decreases again for larger grains

406   with increasing particle size (Wyss et al., 2016b); this provides qualitative support for the existence of the two power law

407   relations. A similar behaviour could be observed only for the calibration measurements at the Urslau stream in Austria

408   (Kreisler et al., 2017). In contrast, calibration measurements from six other sites, including the Ruetz stream, do not show

409   evidence for the existence of similar two–range power law calibration relations.

410   Amplitude information from the geophone signal was recorded in minute intervals at the Fischbach and Ruetz by

411   summing impulse counts separately for different amplitude classes (so-called AH data). Since signal amplitude correlates

412   with grain size at several SPG sites (Wyss et al., 2016a, 2016b, 2016c), this information was used to estimate the grain size

413   distribution for the bedload samples from the Fischbach and Ruetz. It was found that the observed coarsening of the grain

414   size distribution with increasing bedload flux could be qualitatively reproduced from the geophone signal using the AH data.

415   For smaller discharges at the Fischbach and Ruetz, in particular during the winter time, it was found that many

416   implausible geophone impulse counts were recorded. Both SPG measuring sites are situated very close to local roads with

417   regular traffic. The roads are only about half the stream width away from the steel plates, and we therefore identified vehicle

418   traffic as a likely source for the implausible geophone impulses. This is indirectly supported by a comparison with other SPG

419   sites in Switzerland. At most of these sites only very few implausible geophone impulse counts were recorded in the past,

420 which is probably due to the fact that the local roads are farther away from the steel plates, generally at least once or twice
421 the stream width.

422 **6. Data availability**

423 The data cannot be made publicly available for the time being since it is used by the Tyrolean Hydropower Company
424 TIWAG, the owner and provider of the data, in an ongoing hydropower project authorisation procedure.

425 **7. Appendix A: Summary of the amplitude histogram method of Wyss et al. (2016a)**

426 Information about the grain–size distribution of the transported bedload over a Swiss geophone plate can be determined
427 using the number of impulses per amplitude class (called amplitude histogram method). Amplitude histograms (AH data)
428 can be interpreted as a statistical distribution of the signal's amplitude over a given time interval. Using the number of
429 bedload particles per unit mass, absolute bedload masses for each grain–size class were calculated for the Erlenbach stream
430 in Switzerland.

431 For j grain size classes an amplitude threshold value A_{th} (upper class boundary value, in V) corresponds to a threshold
432 particle size D in (mm) separating the grain size class (Wyss et al. 2016a). In this study an empirical relation given in Wyss
433 et al. (2016c) was used (see also Table 2):

434 $D = 85.5\,A_{th}^{0.41}$ $\hspace{8cm}$ (A1)

435 Wyss et al. (2016a) assumed that the number of impulses per amplitude class, IMP_j, are related to the number of particles in
436 the corresponding grain size class, N_j, with a mean weight, G_{mj}, by a coefficient α_j determined from the bedload samples, as
437 follows:

438 $IMP_j = \alpha_j,\,N_j$ $\hspace{8cm}$ (A2)

439 For the calibration of the method for the Erlenbach 31 bedload samples were used. The analysis resulted in the following
440 empirical power law relation between α_j and the class mean grain size D_{mj} in [mm] where the median value of α_j of all
441 bedload samples was used to determine the empirical relation (A3):

442 $\alpha_j = 0.0093\,D_{mj}^{1.09}$ $\hspace{8cm}$ (A3)

443 where the coefficient 0.0093 has the units [mm$^{-1.09}$]. Finally, to estimate the bedload mass per grain size class, the following
444 relation can be used:

445 $M_{est} = N_j\,G_{mj} = \dfrac{IMP_j\,G_{mj}}{\alpha_j}$ $\hspace{7cm}$ (A4)

446 The above procedure was used to estimate the bedload mass for each calibration sample from the Fischbach and the Ruetz,
447 as reported in section 4.1 in the Discussion. To determine the mean weight, G_{mj} in [g] for each grain size class with D_{mj} in
448 [mm], the following empirical relations were used, based on investigations reported in Wyss et al. (2016c):

449 $G_{mj} = 0.00165\, D_{mj}^{2.94}$ for the Fischbach (A5)

450 $G_{mj} = 0.00111\, D_{mj}^{3.03}$ for the Ruetz (A6)

451 Considering Eqs. (A5) or (A6) together with Eqs. (A3) and (A4) it follows that the mass of grains per class is approximately
452 proportional to $IMP_j \bullet D_{mj}^2$. We used this proportionality in section 3.2 to estimate the GSD for the calibration measurements
453 from the Fischbach and Ruetz based on the recorded AH data. The main uncertainty in transferring the method of Wyss et al.
454 (2016a) determined for the Erlenbach to another site is the use of Eq. (A3) which may different at other sites. We used the
455 entire procedure reported here, including Eq. (A3) with the coefficient and exponent determined from the Erlenbach
456 measurements, in section 4.1 to explicitly estimate the total bedload mass for each calibration measurement from the
457 Fischbach and Ruetz based on the recorded AH data.

458 **8. Supplement link**

459 → see also Supplementary Material

460 **9. Author contribution**

461 BF was the main responsible for the concept and installation of the SPG system at the Fischbach and Ruetz. He had
462 suggested to record the AH data as a memory efficient way to extract grain–size relevant information from the raw geophone
463 signal. DR was responsible for the analysis and wrote the paper. Support of colleagues for figure preparation is
464 acknowledged below.
465

466 **10. Acknowledgements**

467 We are grateful to the Tyrolean Hydropower Company (TIWAG) for having performed the geophone calibration
468 measurements in the Fischbach and Ruetz streams and for having provided these data and the continuous geophone
469 measurements to WSL for further analysis. The study was supported by SNF grants 200021_124634 and 200021_137681.
470 We thank Nicloas Steeb, Philipp von Arx, and Thomas Weninger for help with the preparation of some figures; TW also
471 performed grain size analyses of the streambed surface.
472

11. References

Ancey, C., Bohorquez, P., and Bardou, E.: Sediment transport in mountain rivers, ERCOFTAC Bulletin, 100, 37–52, 2015.

Bänziger, R., and Burch, H.: Acoustic sensors as indicators for bed load transport in a mountain torrent, in: Hydrology in Mountainous Regions I, IAHS. Publ. no. 193, pp. 207–214, 1990.

Barrière, J., Krein, A., Oth, A., and Schenkluhn, R.: An advanced signal processing technique for deriving grain size information of bedload transport from impact plate vibration measurements, Earth Surf. Proc. Land., 40, 913–924, 2015a.

Barrière, J., Oth, A., Hostache, R., and Krein, A.: Bed load transport monitoring using seismic observations in a low–gradient rural gravel bed stream, Geophys. Res. Lett., 42, 2294–2301, 2015b.

Barton, J. S., Slingerland, R. L., Pittman, S., and Gabrielson, T. B.: Monitoring coarse bedload transport with passive acoustic instrumentation: A field study, in: U.S. Geological Survey Scientific Investigations Report 2010–5091, 38–51, available at: https://pubs.usgs.gov/sir/2010/5091/papers/listofpapers.html, 2010.

Bassett, C., Thomson, J., and Polagye, B.: Sediment–generated noise and bed stress in a tidal channel, J. Geophys. Res. Oceans, 118, 2249–2265, 2013.

Bathurst, J. C., Graf, W. H., and Cao, H. H.: Bed load discharge equations for steep mountain rivers, in: Sediment transport in gravel–bed rivers, Wiley & Sons, New York, USA, 453–477, 1987.

Beylich, A. A., and Laute, K.: Combining impact sensor field and laboratory flume measurements with other techniques for studying fluvial bedload transport in steep mountain streams, Geomorphology, 218, 72–87, 2014.

Camenen, B., Jaballah, M., Geay, T., Belleudy, P., Laronne, J. B., and Laskowski, J. P.: Tentative measurements of bedload transport in an energetic alpine gravel bed river, in: River Flow 2012, Taylor & Francis Group, London, 379–386, 2012.

Gomez, B.: Bedload transport, Earth–Sci. Rev., 31, 89–132, 1991.

Goto, K., Itoh, T., Nagayama, T., Kasai, M., and Marutani, T.: Experimental and theoretical tools for estimating bedload transport using a Japanese pipe hydrophone, Int. J. Erosion Control Enginering, 7(4), 101–110, 2014.

Gray, J. R., Laronne, J. B., and Marr, J. D. G.: Bedload–surrogate Monitoring Technologies, U.S. Geological Survey Scientific Investigations Report 2010–5091, 37p., available at: http://pubs.usgs.gov/sir/2010/5091/, 2010.

Fehr, R.: A method for sampling very coarse sediments in order to reduce scale effects in movable bed models, in Proceedings of IAHR Symposium on Scale Effects in Modelling Sediment Transport Phenomena, 383–397, Toronto, Canada, 1987.

Habersack, H., Kreisler, A., Rindler, R., Aigner, J., Seitz, H., Liedermann, M., and Laronne, J. B.: Integrated automatic and continuous bedload transport monitoring in gravel bed rivers, Geomorphology, 291, 80-93, 2017.

Hegg, C., McArdell, B. W, and Badoux, A.: One hundred years of mountain hydrology in Switzerland by the WSL, Hydrol. Process., 20, 371–376, 2006.

505 Krein, A., Klinck, H., Eiden, M., Symader, W., Bierl, R., Hoffmann, L., and Pfister, L.: Investigating the transport dynamics
506   and the properties of bedload material with a hydro–acoustic measuring system, Earth Surf. Proc. Land., 33, 152–163,
507   2008.

508 Kreisler, A., Moser, M., Aigner, J., Rindler, R., Tritthard, M., and Habersack, H.: Analysis and classification of bedload
509   transport events with variable process characteristics, Geomorphology, 291, 57-68, 2017.

510 Leopold, L. B., and Emmett, W. W.: Bedload and river hydraulics – Inferences from the East Fork River, Wyoming, U.S.
511   Geological Survey Professional Paper 1583, 1997.

512 Mao, L., Carrillo, R., Escauriaza, C., and Iroume, A.: Flume and field–based calibration of surrogate sensors for monitoring
513   bedload transport, Geomorphology, 253, 10–21, 2016.

514 McArdell, B. W., Bartelt, P., and Kowalski, J.: Field observations of basal forces and fluid pore pressure in a debris flow,
515   Geophys. Res. Lett., 34, L07406, doi:10.1029/2006GL029183, 2007.

516 Mizuyama, T., Oda, A., Laronne, J. B., Nonaka, M., and Matsuoka, M.: Laboratory tests of a Japanese pipe geophone for
517   continuous acoustic monitoring of coarse bedload, in: U.S. Geological Survey Scientific Investigations Report 2010–
518   5091, 319–335, available at: https://pubs.usgs.gov/sir/2010/5091/papers/listofpapers.html, 2010a.

519 Mizuyama, T., Laronne, J. B., Nonaka, M., Sawada, T., Satofuka, Y., Matsuoka, M. et al.: Calibration of a passive acoustic
520   bedload monitoring system in Japanese mountain rivers, in: U.S. Geological Survey Scientific Investigations Report
521   2010–5091, 296–318, available at: https://pubs.usgs.gov/sir/2010/5091/papers/listofpapers.html, 2010b.

522 Møen, K. M., Bogen, J., Zuta, J. F., Ade, P. K., and Esbensen, K. Bedload measurement in rivers using passive acoustic
523   sensors, in: U.S. Geological Survey Scientific Investigations Report 2010–5091, 336–351, available at:
524   https://pubs.usgs.gov/sir/2010/5091/papers/listofpapers.html, 2010.

525 Nitsche, M., Rickenmann, D., Turowski, J. M., Badoux, A., and Kirchner, J. W.: Evaluation of bedload transport predictions
526   using flow resistance equations to account for macro–roughness in steep mountain streams, Water Resour. Res., 47,
527   W08513, doi:10.1029/2011WR010645, 2011.

528 Recking, A.: A comparison between flume and field bed load transport data and consequences for surface based bed load
529   transport prediction, Water Resour. Res., 46, W03518, doi:10.1029/2009WR008007, 2010.

530 Recking, A.: An analysis of nonlinearity effects on bed load transport prediction, J. Geophys. Res. Earth Surf., 118, 1264–
531   1281, doi:10.1002/jgrf.20090, 2013.

532 Reid, S. C., Lane, S. N., and Berney, J. M.: The timing and magnitude of coarse sediment transport events within an upland
533   gravel–bed river, Geomorphology, 83, 152–182, 2007.

534 Rickenmann, D.: Sediment load and discharge in the Erlenbach Stream, in: Dynamics and Geomorphology of Mountain
535   Rivers, Lecture Notes in Earth Sciences, 52, 53–66, 1994.

536 Rickenmann, D.: Sediment transport in Swiss torrents, Earth Surf. Proc. Land., 22, 937–951, 1997.

537 Rickenmann, D.: Bedload transport measurements with geophones, hydrophones and underwater microphones (passive
538   acoustic methods), in: Gravel Bed Rivers and Disasters, Wiley & Sons, Chichester, UK, 185–208, 2017a.

539 Rickenmann, D.: Bedload transport measurements with geophones and other passive acoustic methods, J. Hydraul. Eng.–
540   ASCE, 143(6), 03117004-1-14, doi: 10.1061/(ASCE)HY.1943-7900.0001300, 2017b.

541 Rickenmann, D., and McArdell, B. W.: Continuous measurement of sediment transport in the Erlenbach stream using
542   piezoelectric bedload impact sensors, Earth Surf. Proc. Land., 32, 1362–1378, 2007.

543 Rickenmann, D., and McArdell, B. W.: Calibration measurements with piezoelectric bedload impact sensors in the Pitzbach
544   mountain stream, Geodin. Acta, 21, 35–52, 2008.

545 Rickenmann, D., and Fritschi, B.: Bedload transport measurements using piezoelectric impact sensors and geophones, in:
546   U.S. Geological Survey Scientific Investigations Report 2010–5091, 407–423, available at:
547   https://pubs.usgs.gov/sir/2010/5091/papers/listofpapers.html, 2010.

548 Rickenmann, D., Turowski, J. M., Fritschi, B., Klaiber, A., and Ludwig, A.: Bedload transport measurements at the
549   Erlenbach stream with geophones and automated basket samplers, Earth Surf. Proc. Land., 37, 1000–1011, 2012.

550 Rickenmann, D., Turowski, J. M., Fritschi, B., Wyss, C., Laronne, J. B., Barzilai, R. et al.: Bedload transport measurements
551   with impact plate geophones: comparison of sensor calibration in different gravel–bed streams, Earth Surf. Proc. Land.,
552   39, 928–942, 2014.

553 Rickenmann, D., Antoniazza, G., Wyss, C. R., Fritschi, B., and Boss, S.: Bedload transport monitoring with acoustic sensors
554   in the Swiss Albula mountain river, Proc. IAHS, 375, 5-10, doi:10.5194/piahs-375-5-2017, 2017.

555 Rigby, J. R., Kuhnle, R. A., Goodwiller, B. T., Nichols, M. H., Carpenter, W. O., Wren, D. G., and Chambers, J. P.:
556   Sediment–generated noise (SGN): Comparison with physical bed load measurements in a small semi–arid watershed,
557   Paper presented at the 2015 SEDHYD Conference, 19–23 April 2015, Reno, Nevada, USA, available at:
558   http://www.sedhyd.org/2015/, 2015

559 Ryan, S. E., and Dixon, M. K.: Spatial and temporal variability in stream sediment loads using examples from the Gros
560   Ventre Range, Wyoming, USA, in: Gravel–Bed Rivers VI: From Process Understanding to River Restoration, in:
561   Developments in Earth Surface Processes, 11, 387–407, 2008.

562 Schneider, J. M., Rickenmann, D., Turowski, J. M., Bunte, K., and Kirchner, J. W.: Applicability of bed load transport
563   models for mixed–size sediments in steep streams considering macro–roughness, Water Resour. Res., 51, 5260–5283,
564   doi:10.1002/2014WR016417, 2015.

565 Schneider, J. M., Rickenmann, D., Turowski, J. M., Schmid, B., and Kirchner, J. W.: Bed load transport in a very steep
566   mountain stream (Riedbach, Switzerland): Measurement and prediction, Water Resour. Res., 52,
567   doi:10.1002/2016WR019308, 2016.

568 Thorne, P. D.: The measurement of acoustic noise generated by moving artificial sediments, J. Acoustic Soc. America, 78,
569   1013–1023, 1985.

570 Thorne, P. D.: Laboratory and marine measurements on the acoustic detection of sediment transport, J. Acoustic Soc.
571   America, 80, 899–910, 1986.

572 Thorne, P. D.: Seabed generation of ambient noise, J. Acoustic Soc. America, 87, 149–153, 1990.

573 Tsakiris, A. G., Papanicolaou, A. N., and Lauth, T. J.: Signature of bedload particle transport mode in the acoustic signal of a

574   geophone, J. Hydraul. Res., 52(2), 185–204, 2014.

575 Turowski, J. M., Badoux, A., and Rickenmann, D.: Start and end of bedload transport in gravel-bed streams, Geophys. Res.

576   Lett., 38, L04401, doi:10.1029/2010GL046558, 2011.

577 Uchida, T., Okamoto, A., Hayashi, S., Suzuki, T., Fukumoto, A., Yamashita, A., and Tagata, S.: Hydrophone observations of

578   bedload transport in mountainous rivers of Japan, in: Advances in River Sediment Research, Taylor & Francis Group,

579   London, 1749–1796, 2013.

580 Voulgaris, G., Wilkin, M. P., and Collins, M. B.: The in situ passive acoustic measurement of shingle movement under

581   waves and currents: instrument (TOSCA) development and preliminary results, Cont. Shelf Res., 15, 1195–1211, 1995.

582 Wyss, C. R., Rickenmann, D., Fritschi, B., Turowski, J. M., Weitbrecht, V., and Boes, R. M.: Measuring bedload transport

583   rates by grain–size fraction using the Swiss plate geophone signal at the Erlenbach, J. Hydraul. Eng.–ASCE, 142(5),

584   04016003, doi: 10.1061/(ASCE)HY.1943-7900.0001090, 2016a.

585 Wyss, C. R., Rickenmann, D., Fritschi, B., Turowski, J. M., Weitbrecht, V., and Boes, R. M.: Laboratory flume experiments

586   with the Swiss plate geophone bedload monitoring system. Part I: Impulse counts and particle size identification, Water

587   Resour. Res., 52, 7744–7759, doi:10.1002/2015WR018555, 2016b.

588 Wyss, C. R., Rickenmann, D., Fritschi, B., Turowski, J. M., Weitbrecht, V., Travaglini, E., Bardou, E., and Boes, R. M.:

589   Laboratory flume experiments with the Swiss plate geophone bedload monitoring system. Part II: Application to field

590   sites with direct bedload samples, Water Resour. Res., 52, 7760–7778, doi:10.1002/2016WR019283, 2016c.

591

592

593

Table 1. Catchment and channel characteristics at the field sites and range of typical parameters for the conditions during the
595   geophone calibration measurements. The q_b values refer to bedload with $D > 10$ mm.

596

	Fischbach	Ruetz
Catchment parameters		
Drainage area (km^2)	71	28
Maximum elevation (m)	3497	3474
Site elevation (m)	1540	1684
Mean annual precipitation (mm)	1670	1880
% glacier	16	20
Channel parameters (measuring site)		
Gradient over 60 m upstream of geophone site S	1.7	2.5
Stream bed width (m)	8.5	8.5
Bed surface D$_{84}$ (m)	0.26	0.28
Bed surface D$_{50}$ (m)	0.09	0.10
Parameter range for calibration periods		
Period of calibration measurements used in this	2008–2013	2008–2013
No. of calibration measurements used in this study	31	21
Max. unit discharge q$_{max}$ (m^2 s^{-1})	1.97	0.97
Min. unit discharge q$_{min}$ (m^2 s^{-1})	0.56	0.41
Max. mean flow velocity V$_{max}$ (m s^{-1})	2.79	1.88
Min. mean flow velocity V$_{min}$ (m s^{-1})	1.51	1.02
Max. unit bedload transport rate, q$_{b,max}$ (kg s^{-1} m^{-1})	7.20	0.214
Min. unit bedload transport rate, q$_{b,min}$ (kg s^{-1} m^{-1})	0.0050	0.0025
Bedload samples: max. D$_{max}$ (m)	0.350	0.150
Bedload samples: min. D$_{max}$ (m)	0.030	0.050
Bedload samples: max. weight (D > 10mm) (kg)	431	128
Bedload samples: mean weight (D > 10mm) (kg)	70.0	20.6
Sampling duration of calibration measurements (s)	30 – 3600	600 – 3600
Recording interval of geophone summary values during normal flow monitoring (s)	900	900

597

598

599

Table 2. Threshold values of the signal amplitude A used for the impulse count of the amplitude histograms at the Fischbach and Ruetz. To estimate a corresponding particle size D, an empirical relation from Wyss et al. (2016c) was used. D_{mg} is the geometric mean size of each particle class.

A_{th} [V]	0.056	0.079	0.112	0.158	0.224	0.316	0.447	0.631	0.891	1.259	1.778	2.512	3.548	5.012	7.079	10.0	12.0
D [mm]	26.2	30.2	34.8	40.1	46.3	53.3	61.5	70.8	81.5	94.0	108	125	144	166	191	220	237
D_{mg} [mm]		28.1	32.4	37.4	43.1	49.7	57.2	66.0	76.0	87.5	101	116	134	154	178	205	228

604

605

606 **Table 3.** Coefficients, exponents and statistical properties for the calibration relations according to eq. 1, 2, 3, 4, 5. All
607 calibration relations refer to bedload mass with $D > 10$ mm, or unit bedload transport rate $q_{b,p}$ for $D > 10$ mm. In
608 the equations, the units are: M in (kg), $q_{b,p}$ in (kg 0.5^{-1} m^{-1} s^{-1}) and $IMPT$ in (1 0.5^{-1} m^{-1} s^{-1}). Here r^2 is the
609 correlation coefficient between values calculated with the regression relation and the recorded bedload masses.
610 Similarly, in all figures, r^2 is determined between the predicted y–value and the observed y–value (in the linear
611 domain). The relative standard deviation $s_{e,r}$ is determined for the ratios (M_{est}/M) of estimated bedload mass M_{est}
612 calculated with the regression relation and the recorded impulses IMP, divided by the recorded bedload mass M.
613 For the first three relations, the number of calibration measurements (n) are given in Table1, for the other two
614 relations they are listed in this table.
615

	Fischbach	Ruetz	both streams
$M = k_{lin}\ IMP$			
k_{lin}	0.0508	0.0436	
r^2	0.964	0.597	
significance level: probability p	<0.0001	<0.0001	
$s_{e,r}$	0.67	1.38	
$M = k_{pow}\ M^e$			
k_{pow}	0.134	1.40	
e	0.88	0.42	
r^2	0.967	0.576	
significance level: probability p	<0.0001	<0.0019	
$s_{e,r}$	0.78	0.92	
$M = k_{tot}\ IMP$			
k_{tot}	0.0558	0.0547	
r^2	0.964	0.597	
significance level: probability p	<0.0001	<0.0001	
$s_{e,r}$	0.73	1.73	
$q_{b,p} = a_1\ IMPT^{b1}$ for IMPT < 0.48 (0.5^{-1} m^{-1} s^{-1})			
a_1	0.0237	0.0237	0.0237
b_1	0.48	0.48	0.48
n	15	15	30
r^2	0.559	0.790	0.524
significance level: probability p	<0.0001	<0.054	<0.0001
$s_{e,r}$	0.77	1.13	0.98
$q_{b,p} = a_2\ IMPT^{b2}$ for IMPT > 0.48 (0.5^{-1} m^{-1} s^{-1})			
a_2	0.0436	0.0436	0.0436
b_2	1.29	1.29	1.29
n	16	6	22
r^2	0.964	0.517	0.966
significance level: probability p	<0.0001	<0.0001	<0.0001
$s_{e,r}$	0.37	1.71	1.11

616

617 **Table 4.** Comparison of yearly bedload (*YBL*, in t) calculated with two different calibration relations, for the year 2010 and
618   for different ranges of *Q* values. The *YBL* values represent transport over the entire stream width; as only every
619   second steel plate is equipped with a geophone sensor, the loads inferred from the geophone impulses were
620   multiplied by a factor of 2 in this table.

621

Stream	Year	Q range	Yearly bedload YBL-A (t) Eqs. (4,5)	Yearly bedload YBL-B (t) Eq. (1)	YBL-A / YBL-B
Fischbach	2010	all Q (including implausible *IMP* values)	10,800	6,430	1.68
		$Q > 3.5 \ \mathrm{m^3 \ s^{-1}}$	10,600	6,410	1.66
Ruetz	2010	all Q (including implausible *IMP* values)	1,360	621	2.19
		$Q > 1.5 \ \mathrm{m^3 \ s^{-1}}$	1,110	600	1.85

622

623

624
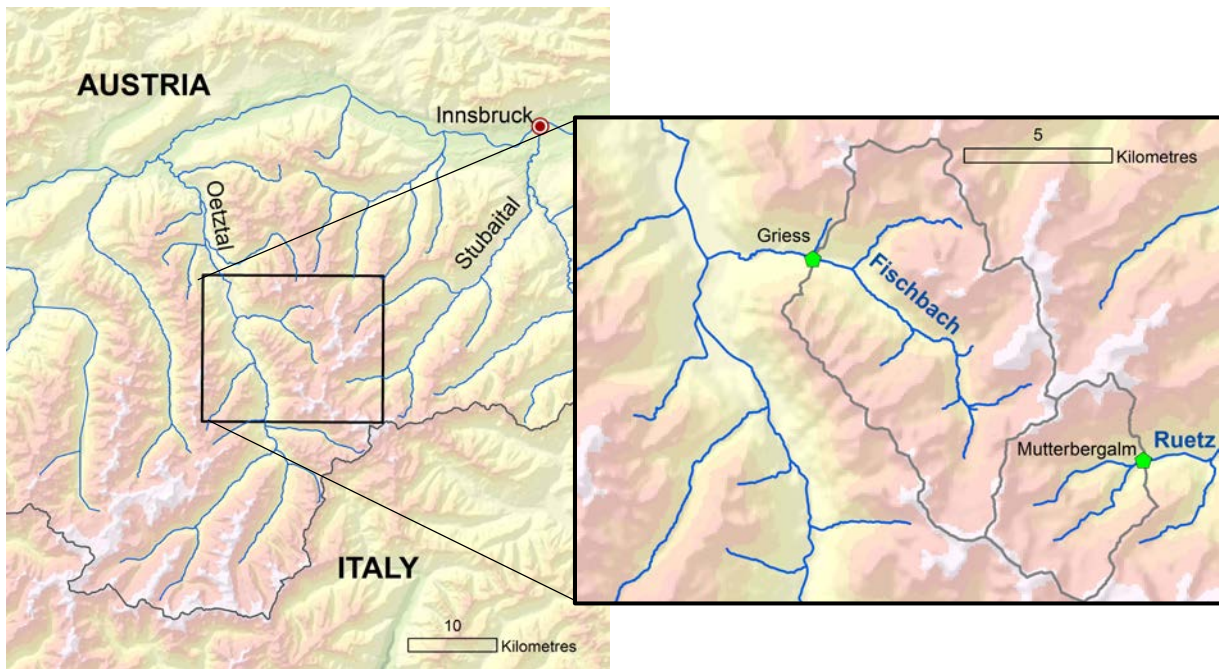
Figure 1. Location of the Fischbach and Ruetz mountain stream catchments in the Stubai Alps of Tyrol in western Austria. The measuring sites are indicated with a green pentagon, and the catchment boundaries are marked with a gray line. (Source of topographic map: Abteilung Geoinformation, Amt der Tiroler Landesregierung; https://www.tirol.gv.at/data)
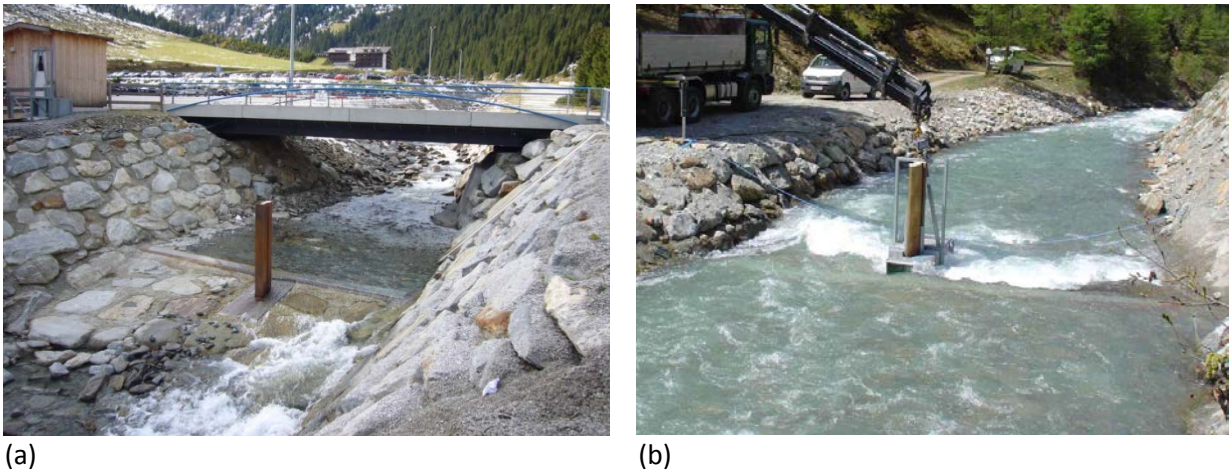
Figure 2. Monitoring sites equipped with a Swiss plate geophone system and a flow gauging station. (a) Ruetz, looking upstream onto the sill with the steel plates (28 October 2009), (b) Fischbach, looking downstream during a calibration measurement using the TIWAG basket sampler (27 May 2008). The steel-concrete pillar visible in both photos is used to guide the positioning of the basket sampler during the collection of bedload samples immediately downstream of the geophone plate.
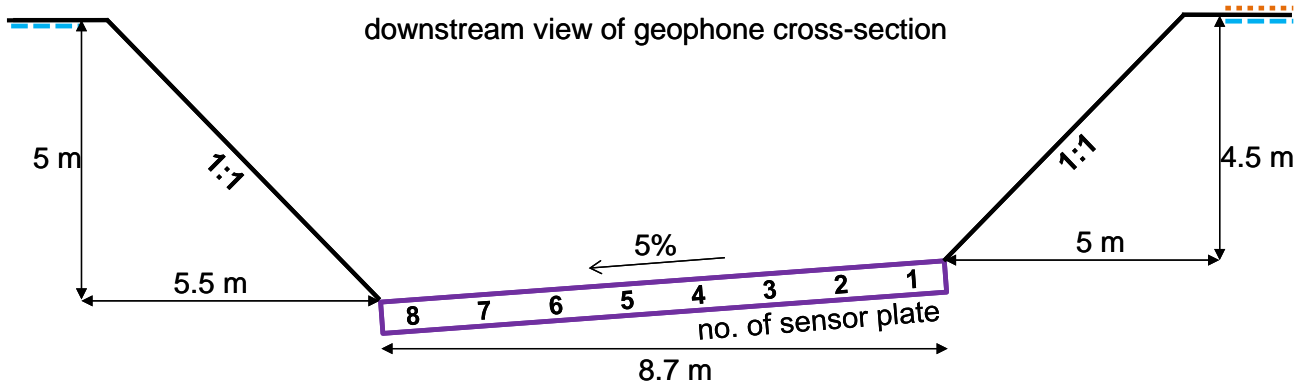
Figure 3. Schematic stream cross-section at the geophone measuring site in both Fischbach and Ruetz. The steel-concrete pillar is located downstream of the sensor plate no. 5. The sill with the steel plates is inclined towards the left bank to improve the resolution of the flow gauge measurements at low discharges. On the banks, the dotted horizontal line indicates the paved local road on river right side at the Fischbach, and the two dashed horizontal lines indicate the graveled parking lot on both river sides at the Ruetz.
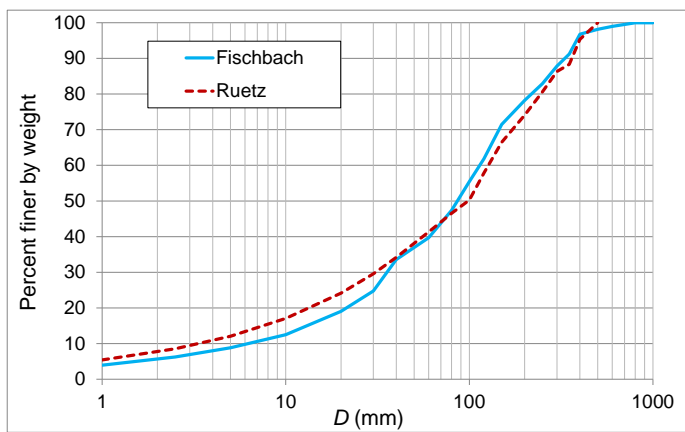
Figure 4. Grain size distribution (GSD) of the surface bed material upstream of the measuring sites. The GSD was measured on 3 October 2012 at the Fischbach and on 4 October 2012 at the Ruetz. The line by number samples included observations for grain sizes $D > 10$ mm, and they were averaged and transformed into a volumetric sample by assuming a 12% unmeasured proportion of $D < 10$ mm (Recking, 2013) and combining it with a Fuller type distribution for the fine material (Fehr, 1987).
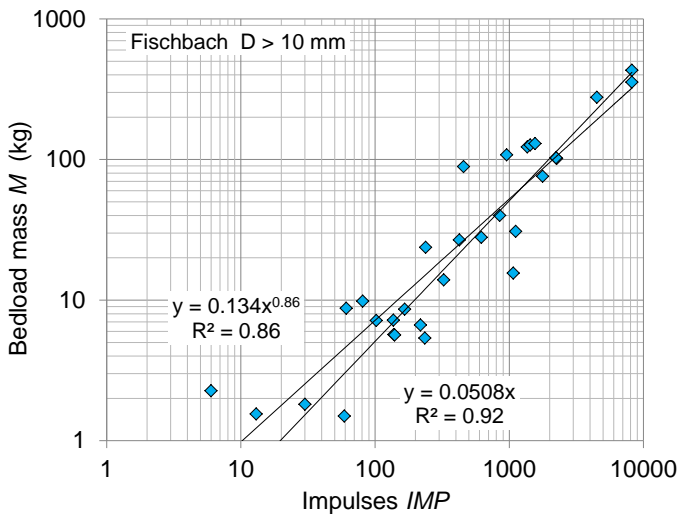
Figure 5. Fischbach: Geophone calibration relationships for grains with $D > 10$ mm between bedload mass M and number of impulses IMP. The linear and power law regression equations are based on 31 calibration measurements for the years 2008-2013.
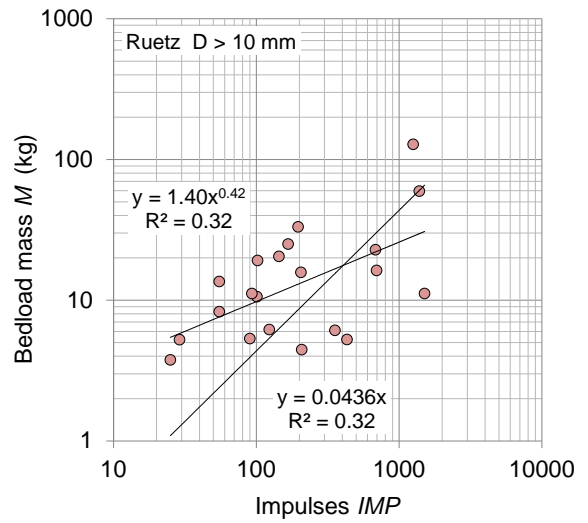
Figure 6. Ruetz: Geophone calibration relationships for grains with $D > 10$ mm between bedload mass M and number of impulses IMP. The linear and power law regression equations are based on 21 calibration measurements for the years 2008-2013.
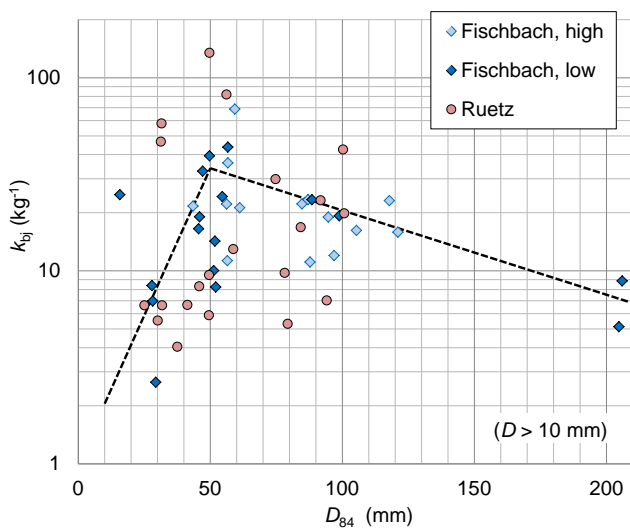
Figure 7. Linear calibration coefficient k_{bj} versus characteristic grain size D_{84}, determined for particles with $D > 10$ mm. Fischbach: data points marked "high" and "low" refer to impulse rates higher and lower than 1 (0.5^{-1} m^{-1} s^{-1}), respectively. The dashed lines are meant to guide the eye.
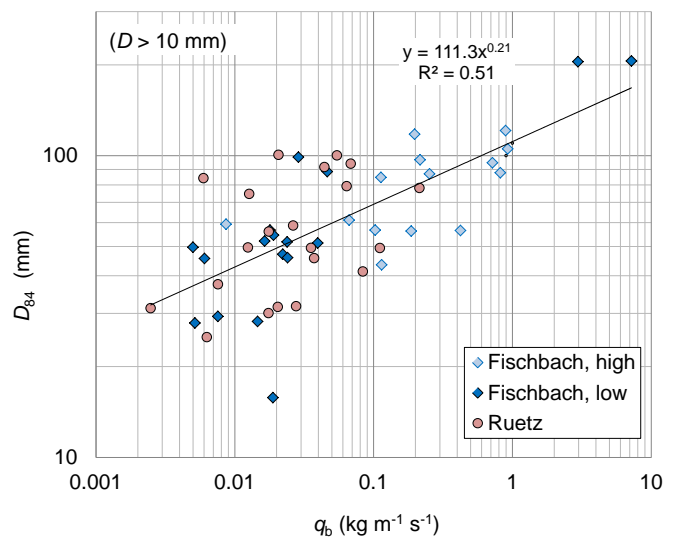
Figure 8. Characteristic grain size D_{84} (determined for particles with $D > 10$ mm) versus bedload flux q_b, derived from the calibration bedload samples (for $D > 10$ mm). Fischbach: data points marked "high" and "low" refer to impulse rates higher and lower than 1 (0.5^{-1} m^{-1} s^{-1}), respectively. The regression line is based on both the Fischbach and Ruetz data.
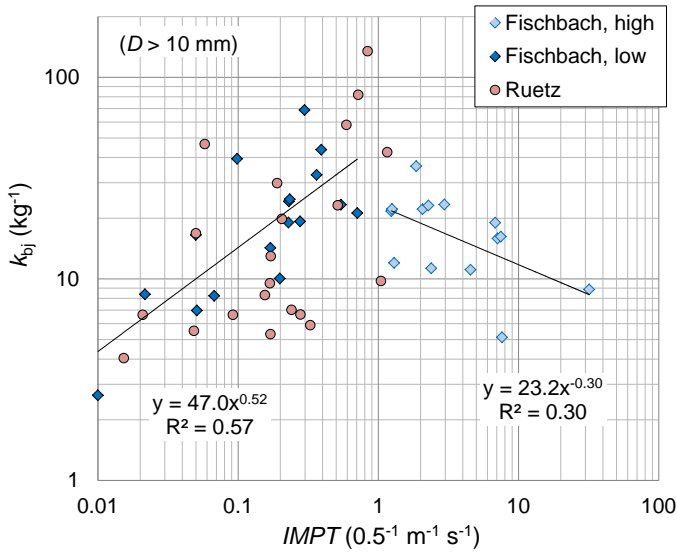
Figure 9. Linear calibration coefficient k_{bj} (for $D > 10$ mm) versus impulse rate *IMPT*. Fischbach: data points marked "high" and "low" refer to impulse rates higher and lower than 1 (0.5^{-1} m^{-1} s^{-1}), respectively. The regression lines are based on the Fischbach data only.
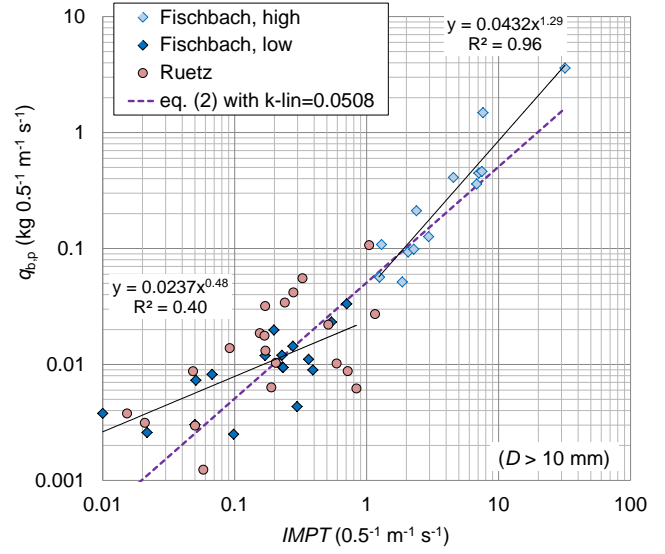
Figure 10. Unit bedload transport rate $q_{b,p}$ for particles $D > 10$ mm vs. impulse rate *IMPT*. Fischbach: data points marked "high" and "low" refer to *IMPT* values higher and lower than 1 (0.5^{-1} m^{-1} s^{-1}), respectively. The regression lines are based on the Fischbach data only. The violet dashed line represents the linear calibration relation Eq. (2) determined for the Fischbach data based on a regression of *M* vs. *IMP*.
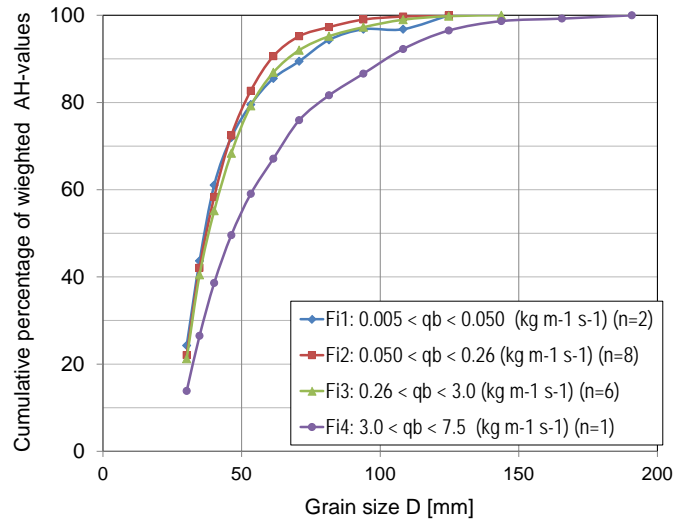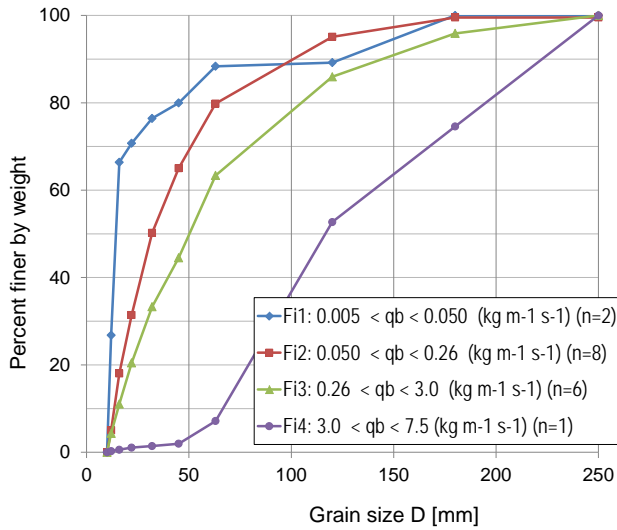
Figure 11. . Fischbach: (a) Grain size distributions derived from the calibration bedload samples (for *D* > 10 mm), averaged for four classes of bedload fluxes q_b (using 17 samples from 2010-2012). (b) Relative distribution of grain sizes estimated from the geophone measurements based on the AH data, averaged for the same four classes of bedload fluxes (using the same 17 sample periods from 2010-2012).
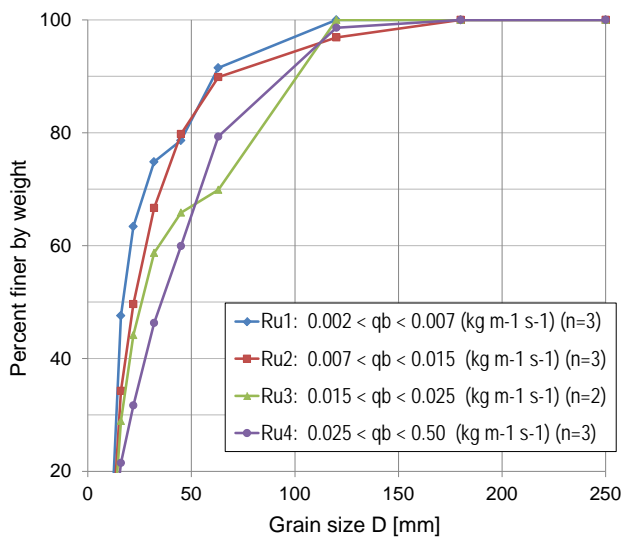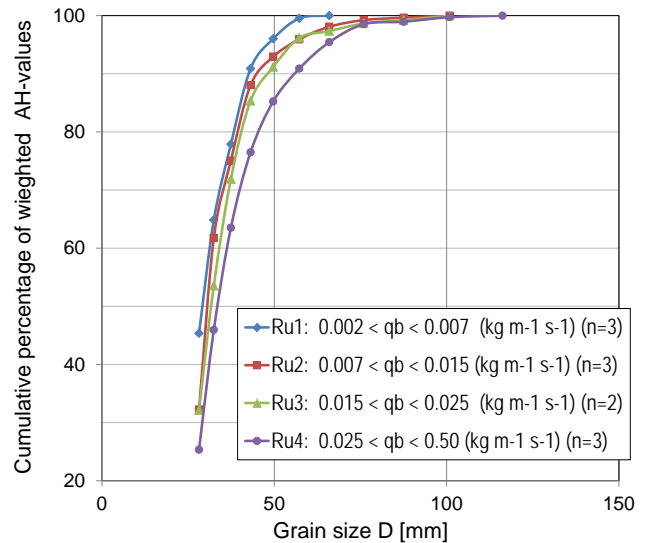
Figure 12. Ruetz: (a) Grain size distributions derived from the calibration bedload samples (for *D* > 10 mm), averaged for four classes of bedload fluxes q_b (using 11 samples from 2010-2013). (b) Relative distribution of grain sizes estimated from the geophone measurements based on the AH data, averaged for the same four classes of bedload fluxes (using the same 11 sample periods from 2010-2013).
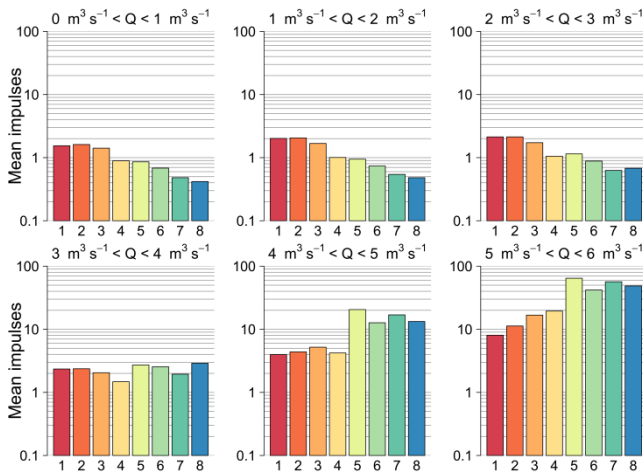
Figure 13. Fischbach: Arithmetic mean of geophone impulses per 15 min for each of the eight plates (ordinates), averaged over the period 2008-2013 and including zero values, for discharge Q classes with width of 1 m^3 s^{-1}, for discharges up to 6 m^3 s^{-1}.
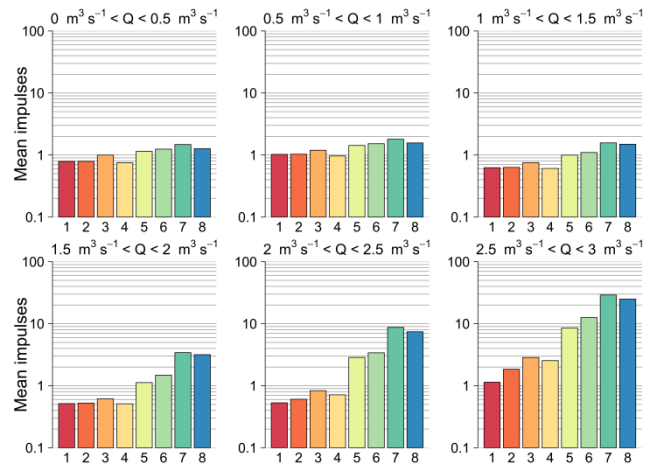
Figure 14. Ruetz: Arithmetic mean of geophone impulses per 15 min for each of the eight plates (ordinates), averaged over the period 2008-2013 and including zero values, for discharge Q classes with width of 0.5 m^3 s^{-1}, for discharges up to 3 m^3 s^{-1}.
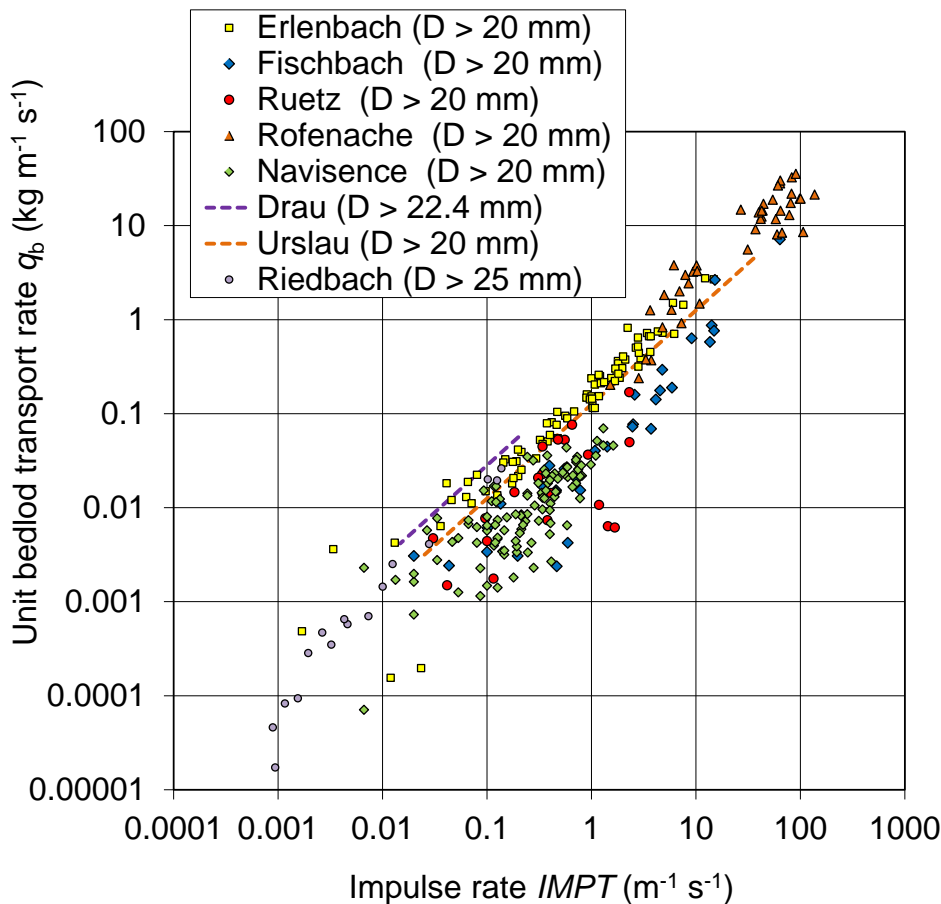
Figure 15. Comparison of geophone calibration data from eight different stream sites. Unit bedload transport rate q_b for particles with D larger than (mostly) 20 mm is plotted against impulse rate *IMPT*. Data sources for additional data are: Wyss et al. (2016c) for Navisence and Erlenbach (some data up to 2016 were added here); regression line from Habersack et al. (2017) for Drau; regression line from Kreisler et al. (2017) for Urslau (linear calibration relation is approximate; q_b values given for D > 10 mm were reduced by factor of 0.68 to estimate q_b values for D > 20 mm; reduction factor was estimated from 85 samples of Erlenbach moving basket data); Schneider et al. (2016) for Riedbach.
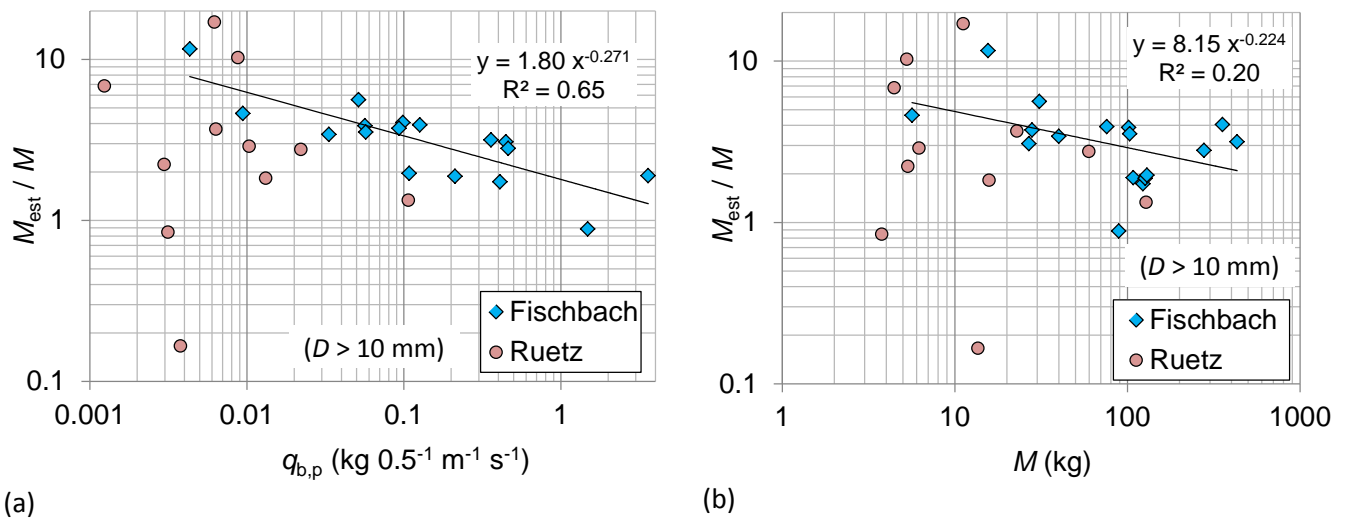
Figure 16. The estimated bedload mass per sample using the method in Wyss et al. (2016a) developed for the Erlenbach, M_{est}, is compared with the measured bedload mass, M, through the ratio M_{est}/M. (a) Ratio M_{est}/M shown vs. unit bedload transport rate $q_{b,p}$ for particles with $D > 10$ mm, (b) Ratio M_{est}/M shown vs. measured bedload Mass M for particles with $D > 10$ mm. In both diagrams the regression line is based on the Fischbach data only.